ISSN 1063-7788, Physics of Atomic Nuclei, 2019, Vol. 82, No. 6, pp. 845–854. © Pleiades Publishing, Ltd., 2019.

ELEMENTARY PARTICLES AND FIELDS
Experiment

Gammas and Charged Particles Identification in Lateral and Additional Apertures of GAMMA-400

I. V. Arkhangelskaja[1)*], A. I. Arkhangelskiy[1),2)], A. M. Galper[1),2)], A. V. Bakaldin[3)], I. V. Chernysheva[1)], E. N. Chasovikov[1)], O. D. Dalkarov[2)], A. E. Egorov[2)], Yu. V. Gusakov[2)], M. D. Kheymits[1)], A. A. Leonov[1),2)], N. Yu. Pappe[2)], M. F. Runtso[1)], Yu. I. Stozhkov[2)], S. I. Suchkov[2)], N. P. Topchiev[2)], and Yu. T. Yurkin[1)]

Received July 19, 2019; revised July 19, 2019; accepted July 19, 2019

Abstract—The GAMMA-400 (Gamma Astronomical Multifunctional Modular Apparatus) will be a new generation satellite gamma-observatory. The gamma-ray telescope GAMMA-400 consists of the anticoincidence system (top and lateral sections—ACtop and AClat), the converter-tracker (C), the time-of-flight system TOF (two sections $S1$ and $S2$), the position-sensitive and electromagnetic calorimeters (CC1 and CC2), the scintillation detectors of the calorimeter ($S3$ and $S4$) and lateral anticoincidence detectors of the calorimeter LD. Two apertures used for observation of transient events do not require the best angular resolution as for the gamma-ray bursts and solar flares from both upper and lateral directions. Additional aperture allows the particle registering from upper direction, which do not interact with converter-tracker and do not form a TOF signal. The lateral aperture allows registering of γ-quanta in perpendicular direction with respect to main axis of GAMMA-400 due to CC2, LD, $S3$, and $S4$. The thickness of CC2 in this direction is $\sim 44\ X_0$ and this allows detection of gammas, electrons and positrons with energies up to 10 TeV. The results of calculation of the fractal dimension of temporal profiles of additional aperture prototype of GAMMA-400 during its calibration using secondary positron beam of the synchrotron C-25P "PAKHRA" of Lebedev Physical Institute confirm the absence of any correlation between the AC and CC1 characteristics and correspondence of additional aperture background to Poisson statistics or Erlang one with shape parameter up to 10.

DOI: 10.1134/S1063778819660049

1. SHORT DESCRIPTION OF GAMMA-400 APERTURES

The gamma-ray telescope GAMMA-400 (Gamma Astronomical Multifunctional Modular Apparatus) consists of the anticoincidence system (top and lateral sections—ACtop and AClat), the converter-tracker (C), the time-of-flight system TOF (two sections $S1$ and $S2$), the position-sensitive calorimeter CC1, the electromagnetic calorimeter CC2, the scintillation detectors of the calorimeter ($S3$ and $S4$), and the lateral anticoincidence detectors of the calorimeter LD. A sketch of the under consideration variant of the gamma-ray telescope GAMMA-400 and its three apertures are shown in Fig. 1. Three sensor types are used in these systems: tracking coordinate detectors, plastic and inorganic scintillators [1, 2]. Double (X, Y) tracking coordinate detectors (marked as CSD in Fig. 1) are used in the converter-tracker (C) and position-sensitive calorimeter CC1. The following detectors are based on BC-408 plastics: the time-of-flight system TOF (two sections $S1$ and $S2$), top (ACtop) and lateral (AClat) sections of anticoincidence system, the scintillation detectors of the calorimeter ($S3$ and $S4$) and the lateral detectors of the calorimeter (LD) (its installation is required for particle registration from lateral directions). All detector systems ACtop, AClat, $S1-S4$, and LD consist of two sensitive layers of 1-cm thickness each [3]. Two calorimeters are made of CsI(Tl): the position-sensitive (CC1) and the electromagnetic (CC2) ones. The thickness of CC1 and CC2 is $\sim 2\ X_0$ ($\sim 0.1\ \lambda_0$) and $\sim 16\ X_0$ ($\sim 0.74\ \lambda_0$), respectively (where X_0 is the radiation length and λ_0 is the nuclear interaction length).

2. THE GAMMA-QUANTA REGISTRATION IN DIFFERENT GAMMA-400 APERTURES

The total calorimeter thickness for vertical incident particles is $\sim 18\ X_0 (\sim 0.8\ \lambda_0)$ [3] (both CC1

[1)]National Research Nuclear University MEPhI (Moscow Engineering Physics Institute), Moscow, Russia.
[2)]P.N. Lebedev Physical Institute of the Russian Academy of Sciences, Moscow, Russia.
[3)]Scientific Research Institute of System Analysis of the Russian Academy of Sciences, Moscow, Russia.
[*]E-mail: irene.belousova@usa.net

and CC2). Laterally incident particles registered by CC2 and for such events calorimeter thickness is $\sim 44\ X_0$ ($\sim 2\ \lambda_0$) [3]. There are two opportunities of particle registration using GAMMA-400: event-by-event mode and spectral one.

The GAMMA-400 is optimized for registration of γ-quanta and charged particles with energy $\sim$100 GeV with the best performance parameters achieved using the main aperture for upper incidents. The size of the main aperture is defined by the geometry of the converter-tracker (C): the gammas converted in tungsten foils are registered. The triggers in the main aperture will be formed using information about the particle direction provided by the TOF system and one about the presence of charged particles or backsplash obtained from the ACtop and AClat anticoincidence detectors in the energy band of $E > 20$ MeV for gammas and $E > 100$ MeV for electrons [4]. The gamma-ray telescope operates in event-by-event registration mode in this aperture.

The other two apertures are used for observation of transient events (gamma-ray bursts—GRBs, soft gamma repeaters (SGR), pulsars, solar flares, etc.) do not require the best angular resolution both from upper and lateral directions.

The additional aperture allows registering particles from upper direction which do not interact with the converter-tracker and do not form a TOF signal. In the additional aperture the gamma-telescope also operates in event-by-event registration mode (see panel (a) in Fig. 2). Particle detection in the additional aperture is triggered by signals from fast discriminators of CC1 individual strips in anticoincidence with TOF [4]. Up–down particle direction can be reconstructed using fast signals from individual strips of detectors CC1 and $S3$, anticoincidence in this aperture is provided by $S2$, LD, and $S4$. In this case, $S2$ and LD are used as anticoincidence detectors, with a larger energy deposition possibly signifying not only the shower propagating beyond the calorimeter, but a particle entering laterally outside of this aperture (and said particle's backsplash). These kinds of events would be undistinguishable within the margin of error. Therefore, only $S4$ is used as a leakage detector in this case, with energy deposition it signifies that the shower propagated beyond CC2. In this case, only a lower limit of the particle energy can be obtained. The analysis of the $S3$ energy deposition shows whether the shower starts propagating in CC1 or not. In this case it is an electromagnetic cascade, because a nuclear cascade starts propagating deeper due to the small CC1 thickness being only $\sim 2\ X_0$ ($\sim 0.1\ \lambda_0$). Moreover, it also gives a rough estimate of the primary particle energy.

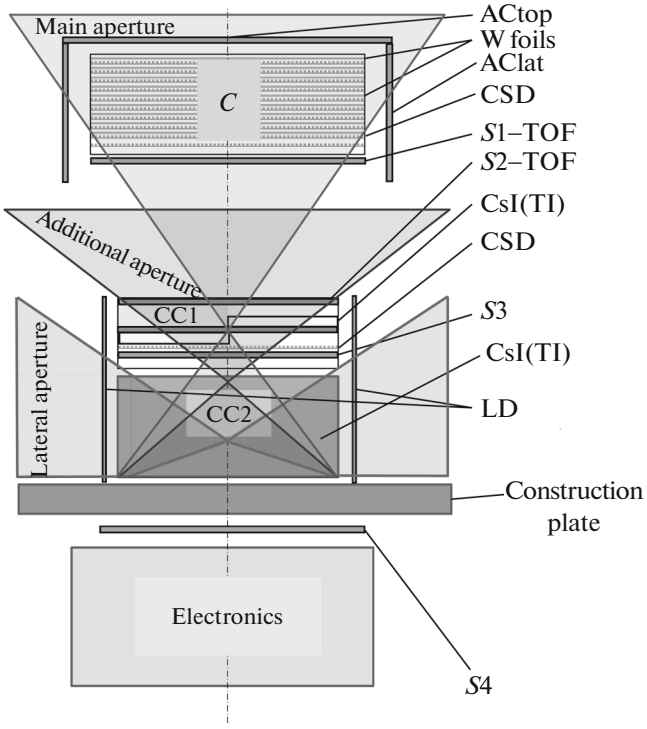

Fig. 1. The sketch of the under-consideration variant of GAMMA-400 telescope [1–3] and its three apertures [4]: main, additional, and lateral. The following detectors are based on BC-408 plastics: the time-of-flight system TOF, the anticoincidence system AC, the scintillation detectors of the calorimeter ($S3$ and $S4$) and the lateral detectors of the calorimeter (LD). The top section of the anticoincidence system ACtop consisst of two layers; each contains 13 strips with dimensions of $128 \times 10 \times 1$ cm^3. The lateral one AClat consists of four detectors and also includes two layers; each contains 13 strips but with size of $60 \times 10 \times 1$ cm^3. The time-of-flight system TOF consists of two detectors $S1$ and $S2$; each includes two layers. The layers of $S1$ contain 10 strips with dimensions of $100 \times 10 \times 1$ cm^3 every, but the ones of $S2$ include 8 strips with dimensions of $80 \times 10 \times 1$ cm^3 each. The scintillation detectors of the calorimeter ($S3$ and $S4$) are similar to $S2$. The lateral detectors of the calorimeter LD are similar to AClat. The position-sensitive calorimeter CC1 consists of two parts, each contains 16 crystals based on CsI(Tl) with dimensions of $40 \times 5 \times 4$ cm^3 ($\sim 2\ X_0$ and $\sim 0.1\ \lambda_0$). The electromagnetic calorimeter CC2 includes 23×23 crystals based on CsI(Tl) with dimensions of $29 \times 3.6 \times 3.6$ cm^3 ($\sim 16\ X_0$ and $\sim 0.74\ \lambda_0$). Double (X, Y) tracking coordinate detectors CSD consist of combination of layers using 100-cm-long scintillating fibres in converter-tracker C and 80-cm-long ones in CC1. Fibres are similar to those used in Scintillating Fibre tracker (SciFi) of upgraded LHCb experiment in CERN [5, 6].

A positron beam with energy of 300 MeV [7] was used for the calibration of prototypes of GAMMA-400 detectors at the synchrotron "PAKHRA". The prototype of the additional aperture of GAMMA-400

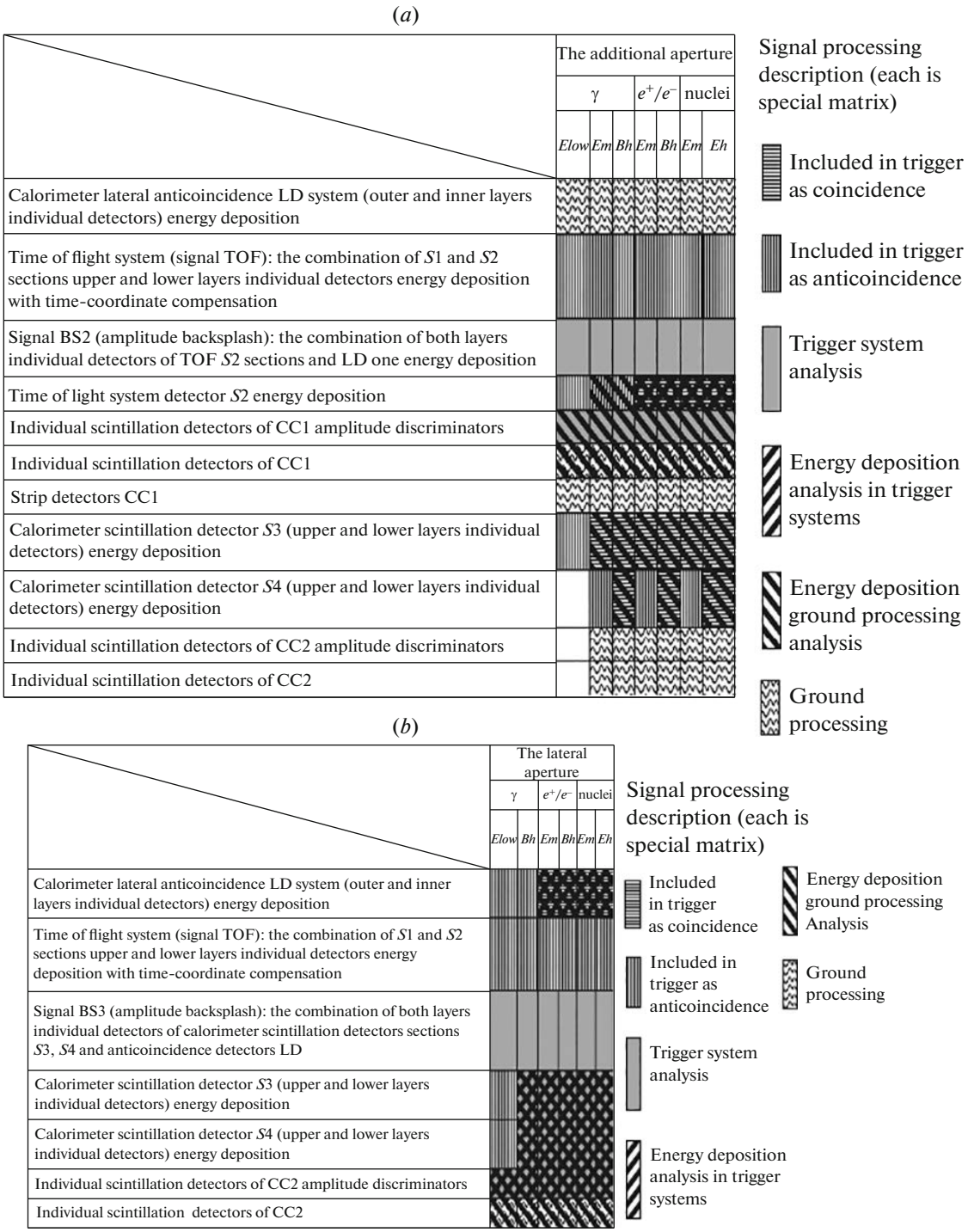

Fig. 2. The detector response analysis matrix for triggers and trigger markers signals formation matrixes for the additional (*a*) and lateral (*b*) apertures (adopted from [4]).

consists of two detectors. One of them is the BC-408-based one with dimensions of $128 \times 10 \times 1$ cm^3 (one detecting strip from the AC prototype) and the other is composed of a CsI(Tl) crystal with dimensions of $33 \times 5 \times 2$ cm^3 (one block of CC1 prototype) [8, 9]. We calculated the fractal dimension of temporal profiles measured during calibrations of the AC/LD and CC1 prototypes. The preliminary results are 1.50 ± 0.05 and 1.48 ± 0.08, respectively [9]. These results confirm the absence of any correlation between these detectors' characteristics and that the background of this aperture obeys Poisson statistics or Erlang one with shape parameter up to 10.

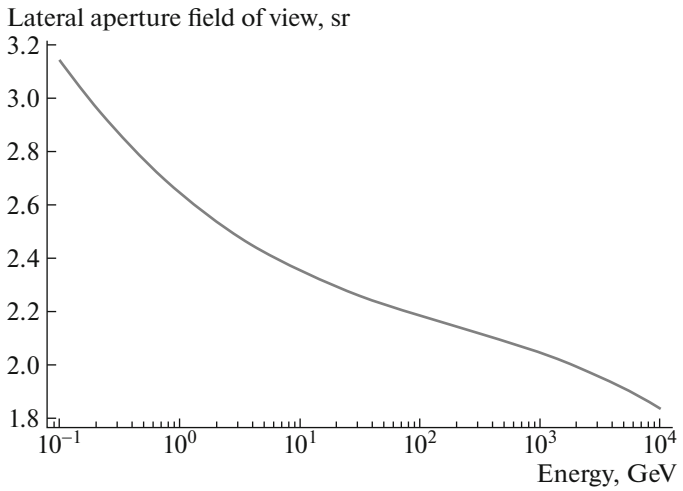

Fig. 3. The dependence of lateral aperture field of view on initial γ-quantum energy.

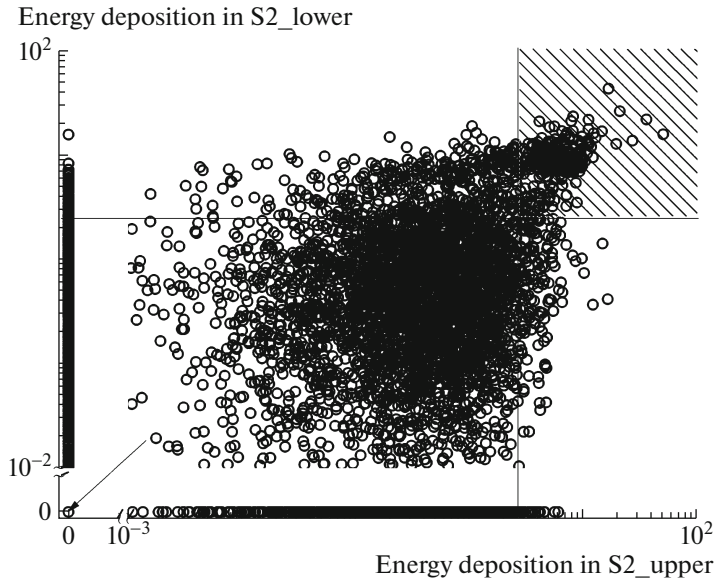

Fig. 4. The results of simulation of total energy deposition distributions in $S2$ (both upper and lower layers) for subsets of 7500 gammas with $E = 3$ GeV. Vertical and horizontal lines together with dashed area represent energy threshold for charged particles registration 2.8 MeV. Approximately 15% of gammas are in this area and be recognized as electrons, but ~85% of γ-quanta can be detected. Arrow marked area contains events with energy deposition less than 1 keV in both $S2$ layers constituted ~70%.

For particle identification only signals from each individual detecting unit of detectors system without any summation are analyzed. Thus, we used individual signals from an ADS placed from two sides of long scintillators. However, backsplash should be taken into account. This effect occurs when low-energy charged particles (mostly electrons from electromagnetic shower) and gammas moved backward relatively to the incident particle due to particle production in their interactions with the detectors and construction materials and reverse scattering of secondary particles. Because of these particles interact with detectors working in anticoincidence mode, the γ quantum could be identified as a charged particle [10]. But backsplash for the γ quantum starts only 1 X_0 after it first interaction. Therefore, even without using the converter, showers for electrons and gammas have different signature. Thus, if gammas were converted at the end of the first 1 X_0, its backsplash was formed only during the second X_0 and should move back through the material of detector and be absorbed. The results of 3-GeV γ-quanta interaction inside $S2$ are presented in Fig. 4. It was confirmed that ~85% of gammas can be detected in additional

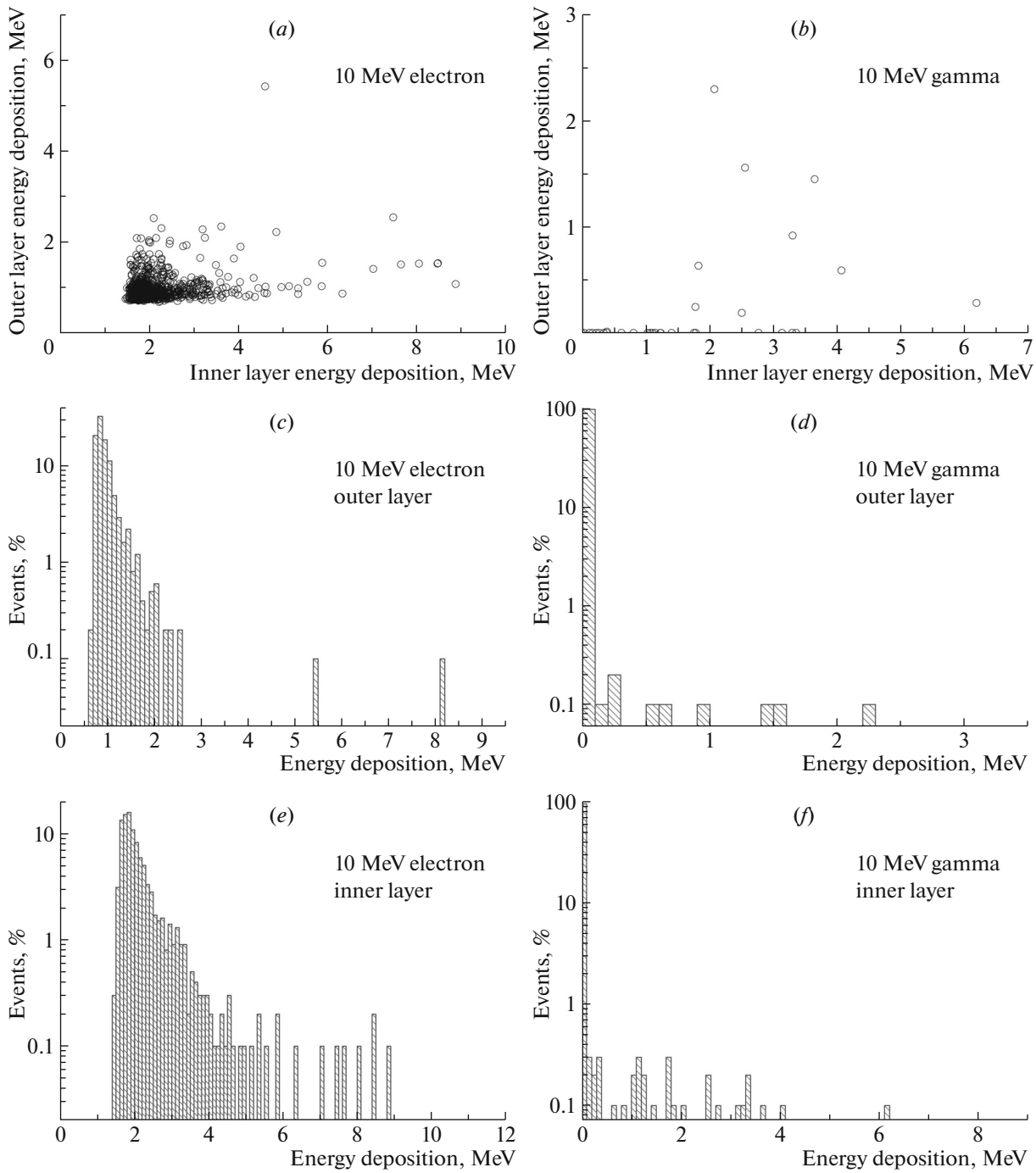

Fig. 5. The comparison of the results from simulations of 10 MeV gammas and electrons energy deposition inside both layers of individual detector of LD which particle incident.

aperture and the backsplash can be effectively rejected using the energy deposition analysis in both layers of $S2$.

The energy band for gamma registration in this aperture in the event-by-event mode is similar to the main one. The angular resolution is provided by the layer of double (X, Y) tracking coordinate detectors in the CC1. The reconstruction of the starting point position of the electromagnetic shower is realized due to the methods analogous to the technique used in accelerator (so-called "center-of-gravity technique") allowing accuracy $\sim$1 mm for electrons (positrons) with $E \sim 8$ GeV—for example, in experiments BTeV [11] and PANDA [12]. The additional aperture can be used in the spectral mode for the study and correction (in addition to main scientific purposes) of the energy

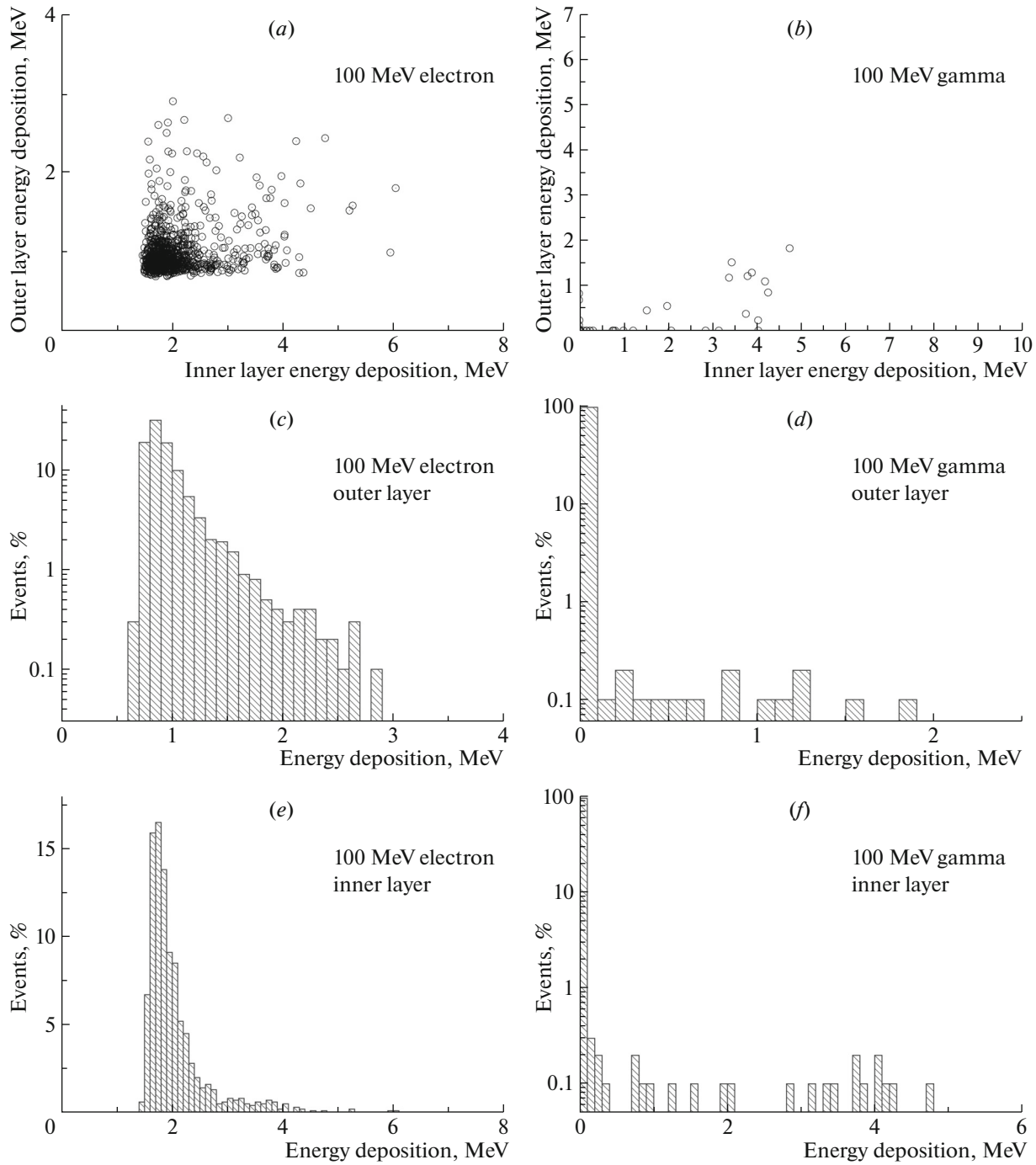

Fig. 6. The comparison of the results from simulations of 100 MeV gammas and electrons energy deposition inside both layers of individual detector of LD which particle incident.

spectra of known source and non-stationary events, such as solar flares, GRBs, SGR, pulsars, etc. in the energy band $E > 1$ MeV. At the same time, the particles' direction determining is possible for low-energy events (the energy range is defined for each event depending on the flux, so the count speed during the count spike length would be at least several standard deviations higher than the background) by comparing count speeds of separate detectors in CC1 similar to BATSE (Burst And Transient Source Experiment onboard Compton Gamma Rays Observatory) algorithm for transient sources (see [13] and references therein) and KONUS detectors [14].

In the cases, where the event entry direction is known and the determination of the position of the high-energy source is not necessary (solar flares,

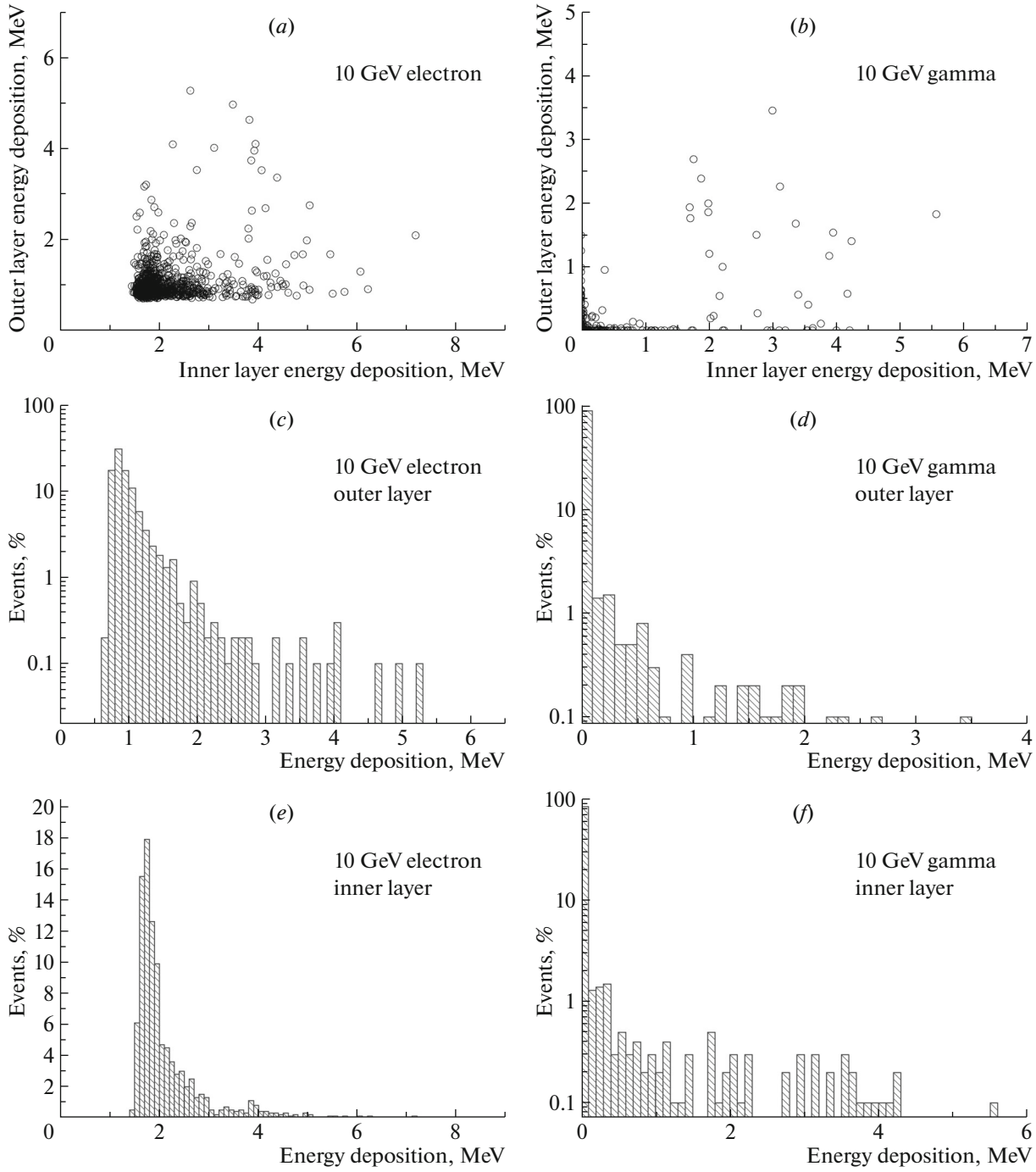

Fig. 7. The comparison of the results from simulations of 10 GeV gammas and electrons energy deposition inside both layers of individual detector of LD which particle incident.

GRBs, SGRs, bright pulsars, etc.), the CC2 lateral aperture can be used to register γ-quanta. The event detection in this aperture is triggered with a signal from fast discriminators of CC2 individual strips in anticoincidence with TOF pulse and CC1 individual strips fast discriminators. The γ-quanta of higher energies can be identified using energy deposition in the individual strips of LD, $S3$, $S4$ and fast signals from discriminators of CC2 individual detectors (see panel (*b*) on Figs. 2). For this aperture, the energy resolution is determined only by CC2 calorimeter, with full effective depth for lateral aperture being $\sim$44 X_0 or $\sim$2.0 λ_0. It allows to increase maximal detectable γ-quanta energy up to several TeV—see lateral aperture field of view dependence on initial γ-quantum energy presented in Fig. 3. The $S2$, $S3$,

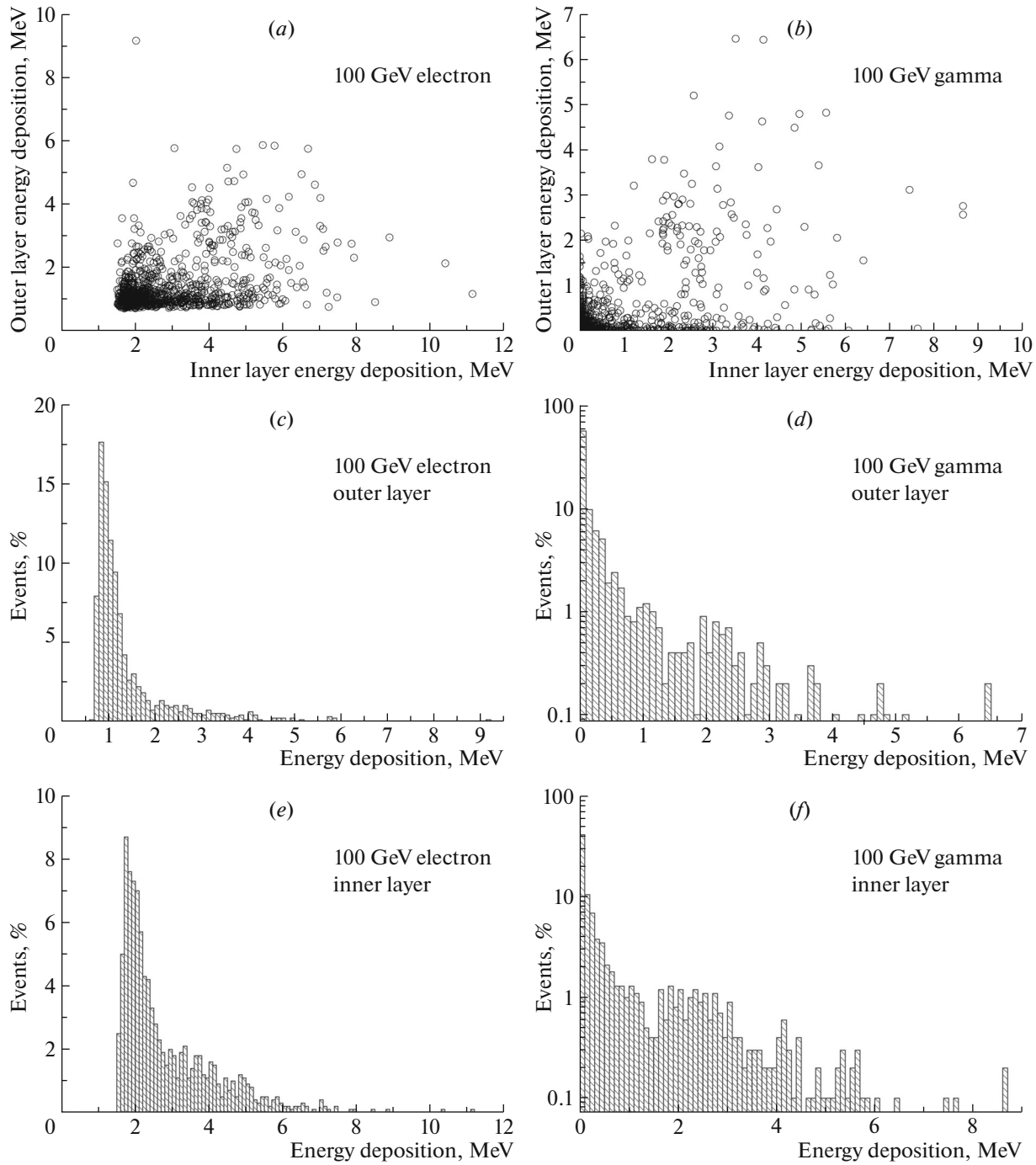

Fig. 8. The comparison of the results from simulations of 100 GeV gammas and electrons energy deposition inside both layers of individual detector of LD which particle incident.

$S4$, and LD detectors are used as anticoincidence detectors, with high-energy deposition in $S2$ indicating primary particle entry from above the aperture. In this case, $S3$ and $S4$ are used as leakage detectors, with high-energy deposition signaling shower egress beyond CC2. The backsplash effect mostly rejected due double layered LD. The results from simulations of gammas and electrons passing through lateral aperture in each layer of individual detector LD which particle incident are shown in Figs. 5–8 for energies of 10 MeV, 100 MeV, 10 GeV, and 100 GeV, respectively. The results of these figures' analysis are presented in Table 1. Using combination of energy thresholds with values of 0.5 and 1.0 MeV it is possible to provide a detector efficiency of ~96% for gammas in the energy band of 10–100 MeV and

Table 1. Trigger activation probability for γ-quanta in lateral aperture

Energy deposition threshold		Trigger activation probability for γ-quantum of a given energy			
Outer layer, MeV	Inner layer, MeV	10 MeV	100 MeV	10 GeV	100 GeV
0.5	0.5	96%	96%	90%	60%
0.5	1.0	96%	97%	92%	66%
1.0	0.5	96%	96%	92%	64%
1.0	1.0	96%	97%	93%	71%

$\sim$92% at $E \sim 10$ GeV. Only 60% of γ-quanta will be registered at $E \sim 100$ GeV but it is possible to increase this value up to $\sim$70% due to LD energy resolution improvement.

Low-energy photons are recognized by simple anticoincidence signals from the individual detectors of LD and registered in the spectral mode with acquisition time scaled depending on the count rate of the detectors. The angular resolution will be $\sim 5^\circ$ vertical segments only for the γ-quanta with energies of 0.2–10 MeV in the lateral aperture obtained from the CC2 individual detectors count rate analysis for non-stationary events only (GRB and so on). The applied method looks like the KONUS [11] and the BATSE algorithm for transient sources (see [11] and references therein). One side of the calorimeter will be solar oriented to support solar panels functioning and cooling radiator located from its other three sides. It allows to use a part of lateral aperture for solar flares investigation.

3. CONCLUSION

The gamma-ray telescope GAMMA-400 consists of an anticoincidence system (top and lateral sections—ACtop and AClat), the converter-tracker (C), the time-of-flight system (two sections $S1$ and $S2$), the position-sensitive calorimeter CC1, the electromagnetic calorimeter CC2, the scintillation detectors of the calorimeter ($S3$ and $S4$) and the lateral anticoincidence detectors of the calorimeter LD. The two apertures used for observation of the transient events do not require best angular resolution as gamma-ray bursts and solar flares from both upper and lateral directions. The additional aperture allows particle detection from upper directions, which do not interact with converter-tracker and do not form a TOF signal. The results of simulation of 3 GeV γ-quanta interaction inside the double-layered $S2$ confirm that $\sim$85% of gammas can be registered in the additional aperture and backsplash is effectively rejected using energy deposition analysis in both layers of $S2$.

The lateral aperture allows registering γ-quanta incident in perpendicular direction with respect to the main axis of GAMMA-400 due to CC2, LD, $S3$ and $S4$. The thickness of CC2 in this direction is $\sim 44\ X_0$ and it allows the detection of gammas, positrons and electrons with energies up to 10 TeV. The field of view of the gamma-ray telescope varies from 3.1 sr (at $E \sim 0.1$ GeV) down to 1.8 sr (at $E \sim 10$ TeV). Using combination of LD energy thresholds with values of 0.5 and 1.0 MeV it is possible to provide backsplash rejection and a detector efficiency of $\sim$96% for gammas in the energy band of 10–100 MeV and $\sim$92% at $E \sim 10$ GeV. Only 60% of γ-quanta will be registered at energy $\sim$100 GeV but it is possible to increase this value up to $\sim$70% due to LD energy resolution improvement.

We have calculated the fractal dimension of temporal profiles measured during calibrations of the AC/LD and CC1 prototypes using positron beam of the synchrotron C-25P "PAKHRA" of Lebedev Physical Institute. Preliminary results confirm the absence of any correlation between these detectors' characteristics and correspondence of the additional aperture background to the Poisson statistics or Erlang one with shape parameter up to 10.

ACKNOWLEDGMENTS

Authors thank for the support from National Research Nuclear University MEPhI in the framework of the Russian Academic Excellence Project (contract no. 02.a03.21.0005, 27.08.2013).

REFERENCES

1. N. P. Topchiev, A. M. Galper, V. Bonvicini, O. Adriani, R. L. Aptekar, I. V. Arkhangelskaja, A. I. Arkhangelskiy, L. Bergstrom, E. Berti, G. Bigongiari, S. G. Bobkov, E. A. Bogomolov, M. Boezio, M. Bongi, S. Bonechi, S. Bottai, et al., Bull. Russ. Acad. Sci. Phys. **79**, 417 (2015).
2. A. M. Galper, O. Adriani, R. L. Aptekar, I. V. Arkhangelskaja, A. I. Arkhangelskiy, M. Boezio, V. Bonvicini, K. A. Boyarchuk, Yu. V. Gusakov, M. O. Farber, M. I. Fradkin, V. A. Kachanov,

V. A. Kaplin, M. D. Kheymits, A. A. Leonov, F. Longo, et al., Adv. Space Res. **51**, 297 (2013).
3. A. A. Leonov, A. M. Galper, N. P. Topchiev, A. V. Bakaldin, O. D. Dalkarov, E. A. Dzhivelikyan, A. E. Egorov, M. D. Kheymits, V. V. Mikhailov, P. Picozza, R. Sparvoli, S. I. Suchkov, Yu. T. Yurkin, and V. G. Zverev, Adv. Space Res. **63**, 3420 (2018).
4. I. V. Arkhangelskaja, A. I. Arkhangelskiy, E. N. Chasovikov, A. M. Galper, M. D. Kheymits, A. E. Murchenko, and Y. T. Yurkin, J. Phys.: Conf. Ser. **675**, 032015 (2016).
5. P. Hopchev, in *Proceedings of the Fifth Annual LHCP* (Shanghai, China, 2017), arXiv: 1710.08325v1 (2017).
6. A. Obłąkowska-Mucha and T. Szumlak, Nucl. Instrum. Methods A **824**, 62 (2016).
7. G. A. Sokol, T. A. Aibergenov, A. V. Koltsov, A. V. Kravtsov, Yu. I. Krutov, A. I. L'vov, L. N. Pavlyuchenko, V. P. Pavlyuchenko, and S. S. Sidorin, AIP Conf. Proc. **549**, 411 (2000).
8. A. I. Arkhangelskiy, A. M. Galper, I. V. Arkhangelskaja, A. V. Bakaldin, E. N. Chasovikov, I. V. Chernysheva, O. D. Dalkarov, A. E. Egorov, Yu. V. Gusakov, M. D. Kheymits, A. A. Leonov, N. Yu. Pappe, M. F. Runtso, Yu. I. Stozhkov, S. I. Suchkov, et al., J. Phys.: Conf. Ser. (2019) (in press).
9. I. V. Arkhangelskaja, A. I. Arkhangelskiy, E. N. Chasovikov, S. I. Suchkov, M. F. Runtso, Y. T. Yurkin, A. M. Galper, N. P. Topchiev, A. A. Leonov, and A. E. Egorov, J. Phys.: Conf. Ser. **1181**, 012083 (2019).
10. W. B. Atwood, A. A. Abdo, M. Ackermann, W. Althouse, B. Anderson, M. Axelsson, L. Baldini, J. Ballet, D. L. Band, G. Barbiellini, J. Bartelt, D. Bastieri, B. M. Baughman, K. Bechtol, D. Bédérède, F. Bellardi, et al., Astrophys. J. **697**, 1071 (2009).
11. V. A. Batarin, J. Butler, A. A. Derevschikov, Y. M. Goncharenko, V. N. Grishin, V. A. Kachanov, V. Y. Khodyrev, A. S. Konstantinov, V. I. Kravtsov, Y. Kubota, Y. A. Matulenko, Y. M. Melnick, A. P. Meschanin, N. E. Mikhalin, N. G. Minaev, V. V. Mochalov, et al., Nucl. Phys. B Proc. Suppl. **150**, 262 (2006).
12. P. A. Semenov, Yu. V. Kharlov, A. V. Uzunian, S. K. Chernichenko, A. A. Derevschikov, A. M. Davidenko, Y. M. Goncharenko, V. A. Kachanov, A. S. Konstantinov, V. A. Kormilitsin, Yu. A. Matulenko, A. P. Meschanin, Y. M. Melnick, N. G. Minaev, V. V. Mochalov, D. A. Morozov, et al., Nucl. Instrum. Methods A **598**, 224 (2009).
13. J. Hakkila, Research Reports: NASA/ASEE Summer Faculty Fellowship Program, SEE N91–18967 10-99 (Alabama Univ., 1990).
14. E. P. Mazets and S. V. Golenetskii, Astrophys. Space Sci. **75**, 47 (1981).